npj | genomic medicine

Article

Published in partnership with CEGMR, King Abdulaziz University

https://doi.org/10.1038/s41525-025-00535-y

Somatic reversion in CD137 deficiency correlating with Epstein-Barr virus control and clinical improvement

Laura Batlle-Masó[1,2], Joan Padrosa Pulido[3,4], Anna Esteve-Codina[3,5], Janire Perurena-Prieto[1,2,6,7], Clara Franco-Jarava[8], Aina Aguiló-Cucurull[1,2,6], Mónica Martínez-Gallo[1,2,6,7], Cristina Cea[9], Marta Rodriguez-Aliberas[10], Pere Soler-Palacín[2,11,12], Ferran Casals[13,14,15,16], Sara Redondo Velao[17], Montserrat Torrent[17], Laia Alsina[18,19,20] & Roger Colobran[1,2,6,7,9] ✉

Epstein-Barr virus (EBV) is an oncogenic virus ubiquitous in human populations. CD8 T cells play a crucial role in establishing a strong anti-EBV immune response. Among the various inborn errors of immunity (IEI) showing a restricted vulnerability to EBV, *TNFRSF9* (CD137, 4-1BB) deficiency was described in 2019 in patients with chronic EBV viremia and EBV-associated lymphoproliferative diseases. We here investigated a patient with a history of chronic EBV infection and CD137 deficiency who had previously undergone transplantation from her HLA-identical brother. We found that the brother was also a homozygous carrier of the same *TNFRSF9* variant, explaining the patient's inability to control EBV after transplantation. Remarkably, during a period of spontaneous clinical improvement and EBV control, we detected two somatic variants in the patient, which resulted in the emergence of two independent revertant CD8 T cell clones that accounted for up to 20% of CD8 T cells in peripheral blood. Using single cell RNA sequencing we demonstrated that both revertant clones originated post-transplant from donor-derived cells. We report here the first described case of a somatic reversion phenomenon in *TNFRSF9* deficiency, correlating with clinical improvement and paving the way for future gene therapy strategies for this IEI.

Epstein-Barr virus (EBV), a member of the oncogenic γ-herpes subfamily, is a double-stranded DNA virus with a preferential tropism for B lymphocytes, in which it can establish lifelong latent infection. EBV seroprevalence increases with age, reaching >90% in the human adult population. Most of the EBV-exposed individuals are asymptomatic or experience self-limiting disease, such as infectious mononucleosis in adolescents and young adults, which is typically self-resolved. However, some individuals may experience more severe and even life-threatening manifestations like fulminant mononucleosis, persistent EBV viremia, hemophagocytic lymphohistiocytosis (HLH), chronic active EBV (CAEBV) or the development of different types of EBV-related B-cell lymphomas. The higher frequency and severity of these conditions in immunocompromised individuals highlights the critical importance of the immune system in controlling EBV infection. The immune response that maintains EBV under control is largely dependent on cytotoxic lymphocytes, with CD8 T cells being unequivocally required for a robust anti-EBV immunity[1]. This concept is illustrated by inborn errors of immunity (IEI) that show a restricted vulnerability to EBV[2]. Among them, *TNFRSF9* (also known as CD137 and 4-1BB) deficiency was described in 2019 in patients with chronic EBV viremia. EBV-associated HLH and lymphoma were also present in the majority of patients[3–5]. Upon T cell activation, CD137 is induced and acts as a co-stimulatory receptor increasing T cell proliferation, survival, cytokine production, and cytotoxicity. EBV-specific T cells from CD137-deficient patients show defective expansion in response to EBV-infected B cells[3,5]. We report here the first documented case of somatic reversion in *TNFRSF9*/CD137/4-1BB deficiency.

Results

We report a female patient of Maghrebian origin from consanguineous parents and without a known personal or familial background of interest who, at 12 years of age (year 2012), was first evaluated due to progressive mild pancytopenia and hepatosplenomegaly in the context of EBV infection. Her clinical status rapidly evolved to massive hepatosplenomegaly, pancytopenia, a cavum mass, multiple enlarged lymph nodes in the neck, and elevated EBV viral load in plasma, peaking at 750,000 copies/ml. HLH was diagnosed and treatment was started with ganciclovir, rituximab and

A full list of affiliations appears at the end of the paper. ✉e-mail: roger.colobran@vallhebron.cat

2004 HLH protocol. At that time, all known genetic defects in familial HLH associated genes (*PRF1*, *UNC13D*, *STXBP2* and *STX11*) were ruled out. Due to the refractoriness of the HLH episode, she underwent an allogenic hematopoietic stem cell transplantation (HSCT) from an HLA-identical brother (showing normal NK cell cytotoxicity, normal degranulation assay and perforin expression), obtaining a mixed but stable chimerism. In the following years, she was unable to control EBV viremia, suffering a severe chronic EBV infection with an EBV-associated smooth muscle tumor (EBV-SMT) and recurrent EBV viremia reactivations. At the age of 20 (years 2020–2021) the patient experienced a remarkable improvement in EBV control (<5000 copies/ml) and remained clinically asymptomatic with a good general condition. In the last two years (2023–2025) PET-CT scans showed an increase in lymph node size with higher glucose uptake and an increase in EBV viremia up to 80,000 copies/ml (see Fig. 1 and Table 1 for a summary of clinical and laboratory data). The referring clinicians recommended a second HSCT; however, to date, the patient – who remains in good overall condition – has declined.

In 2019, whole exome sequencing (WES) was performed for the patient using pre-transplant DNA obtained in 2012 from peripheral blood. We found a rare homozygous nonsense variant in the *TNFRSF9* gene (c.730C>T/p.Arg244*; chr1-7920873-G-A) (Fig. 2A). *TNFRSF9* encodes the tumor necrosis factor receptor superfamily member CD137/4-1BB, a co-stimulatory molecule that mediates T cell activation and proliferation[6]. A few months before this finding, three independent groups described the CD137/4-1BB deficiency (autosomal recessive) as a novel IEI associated with immune dysregulation and persistent EBV infection[3–5]. The Arg244* variant found in the patient is present at a very low allele frequency in the general population (MAF = 0.000004, gnomAD v4.1.0) and results in a premature stop codon in exon 9, leading to a truncated protein missing the last 12 amino acids of the CD137 molecule. This variant is predicted to be loss-of-function, as it abrogates the most C-terminal TRAF-binding domain (Fig. 2A), which is essential for inducing the NF-κB signaling pathway[7].

Initially, the segregation study in the family could not be conducted because the parents declined consent for testing additional family members. Given the importance of knowing the genotype of the HSCT donor brother, we sequenced the patient's DNA from peripheral blood to estimate the brother's genotype. At that time (year 2019) the patient presented a mixed chimerism (~50%) in granulocytes and B cells and almost a complete donor chimerism (>90%) in T cells. Sanger sequencing revealed that in the mutation position, there was no trace of the wild type allele, indicating that the brother was probably also homozygous for the Arg244* variant (Fig. 2B). In view of these results, the parents agreed to test the donor brother and homozygosity for the Arg244* variant was confirmed (Fig. 2C). The brother was clinically asymptomatic, although he presented a persistent moderate EBV viremia (~3000 copies/ml). Such a striking case of incomplete clinical penetrance has been previously described in three other families, each of them with two siblings carrying homozygous *TNFRSF9* pathogenic variants, one symptomatic and the other asymptomatic[3]. Therefore, at the time, in the absence of a genetic diagnosis, the patient received an HSCT from a brother carrying the same genetic defect in *TNFRSF9*, which may explain why the patient was unable to control EBV viremia for the 8 years following HSCT.

Intriguingly, in the patient's Sanger sequencing, we observed a small peak in the position immediately following the germline c.730C>T mutation (chr1-7920872-C-G, R1). This peak was confirmed to be present in the patient using two different primer pairs and was absent in her brother (Fig. 2B, C) and three control samples (data not shown), ruling out any potential technical artifact. This small peak corresponded to a guanine, changing the STOP codon (TGA) to a serine (TCA), representing a so-called second-site somatic reversion[8], from the original nonsense mutation (Arg244*) to a missense variant (Arg244Ser). This somatic reversion was not present in the patient before HSCT and it was restricted to blood cells given its absence in the DNA obtained from saliva (Fig. 2D). We isolated T and B cells, showing that the somatic reversion was exclusively present in T cells (Fig. 2E). In T cells, where the somatic reversion was enriched, we found another small but clear peak in the exact position of the Arg244* mutation (chr1-7920873-A-G, R2). This could correspond to a second somatic reversion, in this case a true genetic reversion of the germline mutation site to the wild-type sequence (Fig. 2E). To determine if these two small peaks corresponded to two independent somatic events giving rise to two independent somatic reversions, we performed NGS-based deep amplicon sequencing (DAS) in T cells. Results showed that the patient presented two independent T cell revertants (R1 and R2), since the reads carried either the Arg244* mutation alone or the Arg244* mutation combined with either the R1 or the R2 somatic variant, but no reads carried both R1 and R2 variants (Fig. 2E). The presence of both revertants in the patient's brother was excluded with high confidence through NGS-DAS analysis of blood-derived DNA, performed at a read depth of ~5000x and a detection limit of 1% VAF (variant allele frequency). Isolation and sequencing of $CD4^+$ and $CD8^+$ T cells revealed that both R1 and R2 were CD8 T cell clones (Fig. 1F). Using DNA from previous chimerism tests we were able to trace both revertants back to 2018. We confirmed that R1 and R2 were not present in B cells or neutrophils, and that in the oldest available post-HSCT DNA sample (August 2018), both revertants were already present (Fig. 2G). From 2018 to 2025 we followed the evolutionary dynamics of R1 and R2 by precisely quantifying their frequencies in T cells using DAS (Table 2, Fig. 2H). R1 steadily increased in frequency from 2018 to 2020, reaching a maximum VAF of 16% in T cells, before gradually declining to 6.5% in the last follow-up (June 2025). R2 also increased in frequency from 2018 to 2021, reaching a peak VAF of 7% and remaining relatively stable until the last follow-up (6%, June 2025). Remarkably, the period during which the patient experienced

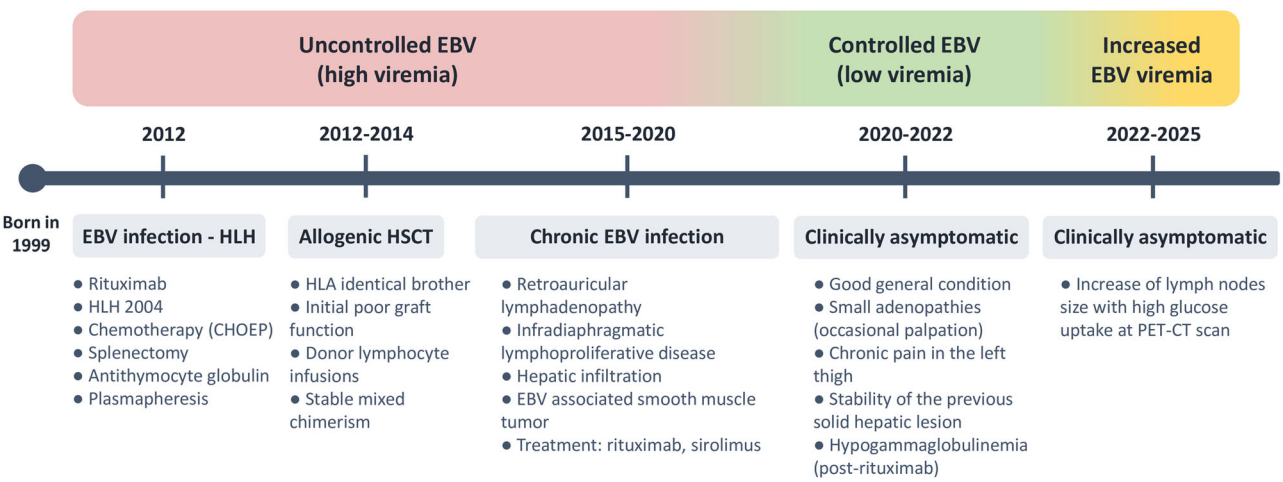

Fig. 1 | Clinical evolution of the patient. A timeline illustrates the key clinical events and the main treatments.

Table 1 | Summary of the patient's laboratory parameters

Date	February 2012	May 2012	November 2015	May 2018	November 2020	November 2023
Episode	EBV infection	HLH episode	EBV reactivation	EBV-associated Smooth Muscle Tumor	Clinically asymptomatic	Clinically asymptomatic
EBV viral load (copies/mL)	15,658	751,100	1352	41,246	3213	10,009
Hemoglobin (g/dL) (12–17)	9.1	9.5	14	15.1	15.1	14.3
Leucocytes (10^3 cells/μL) (4.5–13)	1.6	0.7	6.2	12.8	10.5	11.5
Neutrophils (10^3 cells/μL) (1.5–7)	0.7	0.33	2.39	5.67	2.13	5.9
Lymphocytes (10^3 cells/μL) (1.2–3.5)	0.4	0.35	2.53	5.61	7.32	4.3
Monocytes (10^3 cells/μL) (0–1)	0	0.02	1.06	1.28	0.93	1.2
Platelets (10^3 cells/μL) (140–500)	107	26	321	299	266	338
Lymphocytes subsets						
CD3 + (% lymphocytes) (55–83)	80	85.7	77	92.1	86.4	80.7
CD3 + (10^3 cells/μL) (0.7–2.6)	0.32	0.3	1.95	5.17	0.63	3.47
CD3 + CD4 + (% lymphocytes) (28–57)	60	57.1	35	25.5	29.6	28.3
CD3 + CD4 + (10^3 cells/μL) (0.3–1.4)	0.24	0.2	0.88	1.43	0.22	1.22
CD3 + CD8 + (% lymphocytes) (10–39)	20	22.9	37	62.1	53.7	48.2
CD3 + CD8 + (10^3 cells/μL) (0.2–0.97)	0.08	0.08	0.94	3.48	0.39	2.07
CD4 + /CD8+ Ratio (0.9–3.6)	3	2.50	0.95	0.41	0.55	0.59
CD19 + (% lymphocytes) (5–22)	17	10	15	4.78	3.99	15.27
CD19 + (10^3 cells/μL) (0.1–0.58)	0.068	0.035	0.38	0.27	0.29	0.66
NK CD3-CD56 + (% lymphocytes) (6–31)	4	4	3	1.82	0.91	3.21
NK CD3-CD56 + (10^3 cells/μL) (0.09–0.77)	0.016	0.04	0.076	0.1	0.067	0.14
Treatment	Ganciclovir + IGRT	CHOEP + VP16 + Rituximab Ganciclovir, Meropenem, Splenectomy	No treatment	Sirolimus + Valganciclovir	Valganciclovir	No treatment
PET-CT scan			Liver glucose uptake	Increased liver glucose uptake. Hepatic lymphoproliferation	Stable	Suspected left tight lymphoproliferation

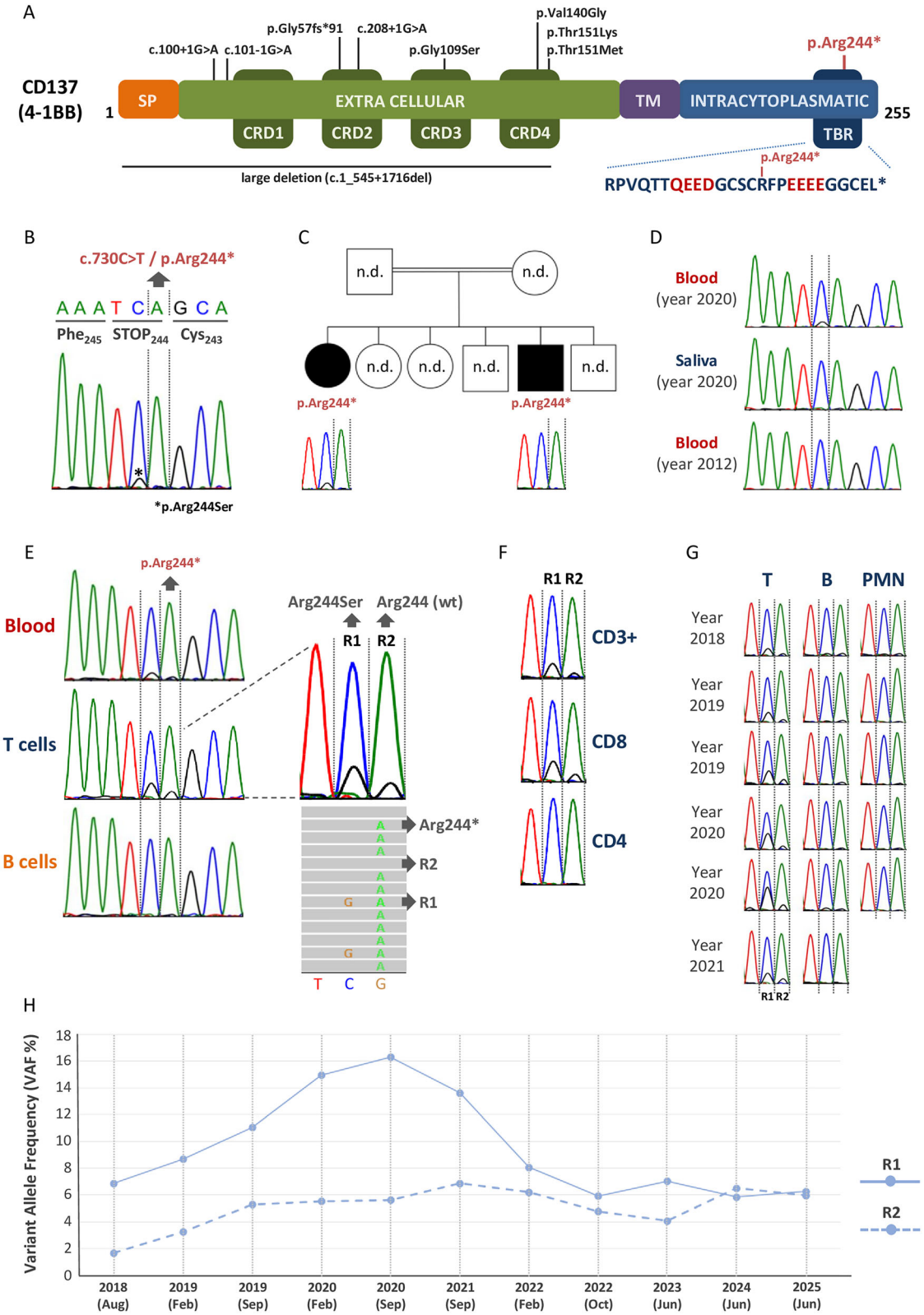

significant clinical improvement and relatively controlled EBV viremia (2020–2021) overlaps with the period in which both revertants reached their maximum VAF.

Finally, since the patient reached an almost complete donor chimerism (>90%) in T cells, we aimed to establish if the cell origin of these revertants was from the patient or her donor. We performed single-cell RNA sequencing (scRNAseq), including T cell receptor (TCR) sequencing, in over 5000 purified CD8 T cells obtained from the patient's peripheral blood (Fig. 3A). *TNFRSF9* expression was observed in 269 $CD8^+$ T cells. Since scRNAseq does not typically sequence the entire transcript, the somatic reversion could be detected only in a few of those cells, but all cells carrying R1 (8 cells) and R2 (3 cells) variants were classified as male cells (XY) based

Fig. 2 | Identification of CD137 deficiency and the somatic reversions. **A** Schematic representation of the CD137 protein. Colored boxes indicate the various domains. All the variants reported to date in the literature are represented in black. The variant identified in the patient (p.Arg244*) and its location in the C-terminal amino acid sequence are displayed in red. Amino acids corresponding to TRAF binding domains are depicted in red. **B** Sanger sequencing of patient's DNA obtained from peripheral blood (year 2019). Reverse sequence is shown. The small peak corresponding to a somatic reversion is indicated by an asterisk. **C** Pedigree and family segregation of the CD137 p.Arg244* variant. The position of the variant in the Sanger sequencing profile is indicated by dashed lines. **D** Sanger sequencing of patient's DNA samples from blood and saliva at different points in time. The position of the somatic reversion is indicated by dashed lines. **E** Sanger sequencing of patient's DNA samples from blood, T cells and B cells. The two independent somatic reversions (R1, R2), exclusively present in T cells, are shown. **F** Sanger sequencing of patient's DNA samples from T cells (CD3+) and purified CD4 and CD8 T cells. The two independent somatic reversions are exclusively present in CD8 T cells. **G** Sanger sequencing of patient's DNA samples from T cells, B cells and polymorphonuclear (PMN) cells at different points in time. **H** Graphical representation of the variant allele frequency (VAF) of both somatic reversions over time.

Table 2 | NGS-based deep amplicon sequencing (NGS-DAS) to quantify the variant allele frequency (VAF) of both somatic revertants (R1 and R2) in different samples and at different time points

Date	Sample (DNA)	Revertant 1 (R1)			Revertant 2 (R2)		
		Read depth (total reads)	Reads R1	VAF (%)	Read depth (total reads)	Reads R2	VAF (%)
2018 (Aug)	T cells	3071	211	**6.8**	2895	48	**1.7**
2019 (Feb)	T cells	11,549	1003	**8.7**	10,837	351	**3.3**
2019 (Sep)	T cells	10,185	1125	**11**	9582	507	**5.3**
2020 (Feb)	T cells	8254	1235	**15**	7742	428	**5.5**
2020 (Sep)	Blood	6621	423	**6.4**	6240	145	**2.3**
	T cells	9904	1615	**16.3**	9292	521	**5.6**
2021 (Sep)	Blood	4880	203	**4.2**	4602	115	**2.5**
	T cells	1578	215	**13.6**	1528	105	**6.8**
2022 (Feb)	T cells	6744	544	**8.1**	6260	389	**6.2**
	CD8 cells	5904	683	**11.6**	5514	444	**8**
2022 (Oct)	Blood	5900	118	**2**	5608	95	**1.7**
	T cells	6569	388	**5.9**	6252	299	**4.8**
	CD8 cells	1481	158	**10.7**	1398	92	**6.6**
2023 (Jun)	Blood	5518	290	**5.3**	5268	123	**2.3**
	T cells	4753	334	**7**	4525	184	**4**
2024 (Jun)	Blood	4770	114	**2.4**	4556	140	**3.1**
	T cells	4537	265	**5.8**	4327	271	**6.2**
2025 (Jun)	Blood	4514	109	**2.4**	4282	91	**2.1**
	T cells	4580	298	**6.5**	4398	262	**6**

For each sample, the total reads and number of reads for each revertant are indicated.
The VAF (%) of the two revertants (R1 and R2) is indicated in bold.

on the expression of genes located outside the pseudoautosomal region of the Y chromosome. Using the TCR sequence, we inferred the presence of R1 or R2 in the remaining cells: 780 cells were classified as R1 and 642 cells as R2 (Fig. 3B). Both R1 and R2 cells corresponded to effector memory RA (TEMRA) CD8 T cells but they were clearly separated in different clusters (Fig. 3B). The global TCR analysis showed that, as expected, only the effector memory CD8 T cells showed hyperexpanded TCRs, whereas naive CD8 T cells contained a diversity of non-expanded TCRs (Fig. 3C). In addition, most R1 and R2 cells contained hyperexpanded TCRs, indicating that the acquisition of somatic reversion probably allowed the original cells to become fully activated and undergo the process of clonal expansion.

Discussion

We reported here the first described case of a somatic reversion phenomenon in CD137/4-1BB deficiency. Although somatic reversion has been documented in other IEI[8,9], to our knowledge, this is the first reported case of somatic reversion occurring post-transplant in HSCT donor cells. Due to the lack of a genetic diagnosis prior to HSCT, the patient received an HSCT from a donor brother who was also homozygous for the same pathogenic variant. Subsequently, at an undetermined time post-transplant, two independent somatic reversions emerged in the donor's CD8 T cells. These two revertant clones likely gained a selective advantage over the cells that did not carry the newly acquired somatic mutations, expanding to the extent that they accounted for up to 20% of CD8 T cells in the blood. Considering that the peak expansion of both revertants overlapped with a marked and apparently spontaneous clinical improvement and EBV control, we hypothesize that the revertant CD8 T cell clones were capable of recognizing EBV-infected cells, becoming activated, and undergoing clonal expansion. Remarkably, after their peak expansion, the overall frequency of the revertant clones decreased and then remained relatively stable over the last 2–3 years. This decline was accompanied by an increase in EBV viral load (from ~3000 to 80,000 copies/ml), although without overt clinical consequences. At present, it is difficult to predict the future dynamics of the revertants or whether the patient will be able to regain control of EBV. This uncertainty has concerned the clinicians to the extent that a second HSCT has been recommended.

Some limitations of this study should be noted. First, we could not directly demonstrate EBV specificity of the revertant clones, namely their recognition of an EBV epitope through the TCR. Second, functional testing of R1 (p.Arg244Ser) was not performed, preventing direct assessment of its effect on functional restoration. Third, the patient received multiple treatments during the study period, including sirolimus, valganciclovir, and rituximab, which need to be considered as potential confounding factors

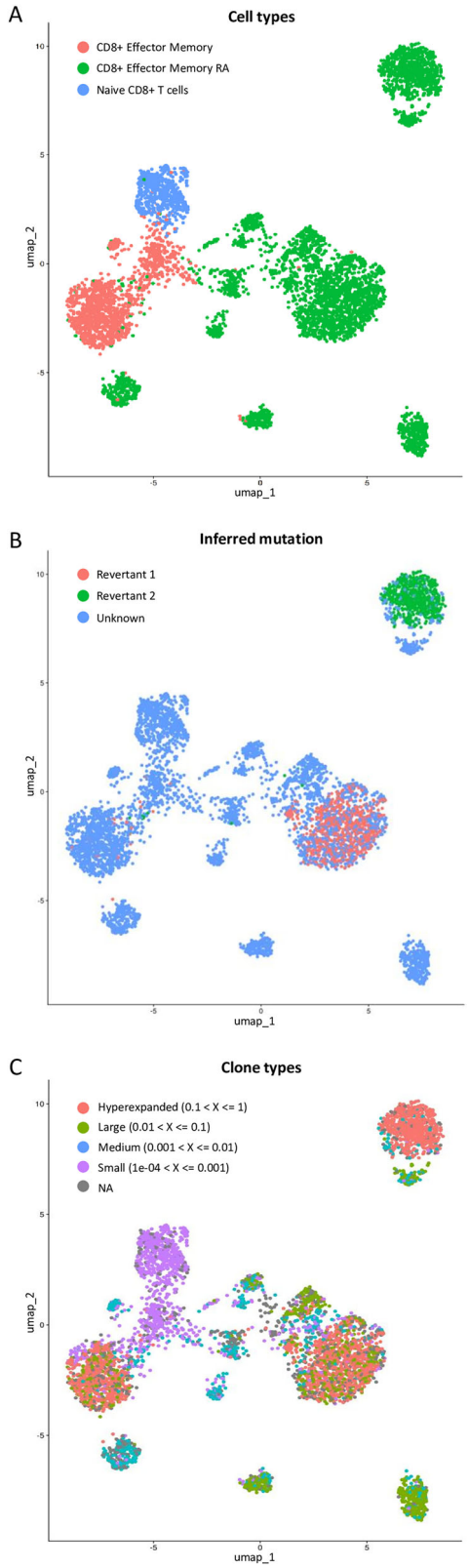

Fig. 3 | Single-cell RNA sequencing of CD8 T cells from patient's blood. A 5463 CD8 T cells were sequenced (586 naïve, 1257 effector memory, and 3620 effector memory RA CD8 T cells). **B** Inference of reversion status in CD8 T cells. To infer the presence of R1 and R2 in cells where the *TNFRSF9* could not be read directly, a T cell receptor (TCR)-based proximity approach was employed. Considering the clonal nature of TCRs, cells presenting the same TCRs were predicted to harbor the same somatic reversion. **C** TCR analysis of CD8 T cells. Cells were classified according to the magnitude of their TCR expansion.

when evaluating the relationship between EBV viremia, clinical evolution, and the dynamics of the revertant clones.

The case reported here represents a fascinating experiment of nature, with the patient's clinical improvement following the emergence of somatic reversions, highlighting a potential path toward gene therapy strategies for CD137/4-1BB deficiency.

Methods

Patients

The patients included in this study were followed at the Hospital Sant Joan de Déu and Hospital de la Santa Creu i Sant Pau (Barcelona, Catalonia, Spain). Written informed consent for the collected samples and analyses reported here, and for publication of the article, was obtained according to the procedures of the local Ethics Committee [code: PR(AG)202/2021]. This study was conducted in full compliance with the Declaration of Helsinki and all relevant ethical regulations for human subjects research.

Sanger sequencing

Genomic DNA was obtained from different samples: peripheral blood (collected in EDTA tubes), saliva and purified cell populations ($CD3^+$, $CD4^+$ T cells, $CD8^+$ T cells, $CD19^+$ B cells and $CD15^+$ polymorphonuclear cells). DNA was isolated using the QIAsymphony SP purification system (Qiagen).

Polymerase chain reaction (PCR) was performed to amplify the regions of interest (primers and PCR conditions are available upon request), and purified PCR products were sequenced on an ABI 3500 DNA Sequencer using the BigDye Terminator sequencing kit 3.1 (Applied Biosystems).

Whole exome sequencing (WES)

Genomic DNA from the patient, obtained prior to HSCT, was used for WES. SeqCap EZ MedExome Target Enrichment Kit (Roche Nimblegen) was used to perform whole-exome enrichment in combination with SeqCap EZ Mitochondrial Genome Design (Roche Nimblegen). The short-insert paired-end libraries for the whole exome capture were prepared with KAPA HyperPrep kit (Roche). In short, 1 microgram of genomic DNA was sheared on a Covaris™ LE220-Plus (Covaris). The DNA fragments were end-repaired, adenylated, and xGen Dual Index UMI Adapters (Integrated DNA Technologies) were ligated. The adaptor-modified end library was enriched by 7 pre-capture PCR and with 14 cycles of post-capture PCR. The size, concentration and quality of the captured material were determined using an Agilent Bioanalyzer DNA 7500 chip.

The WES libraries were sequenced on HiSeq4000 (Illumina) in paired-end mode with a read length of 2 x 101 bp following the manufacturer's protocol for dual indexing. Image analysis, base calling and quality scoring of the run were processed using the manufacturer's software Real-Time Analysis (v2.7.7) and followed by the generation of FASTQ sequence files. The data was mapped and aligned against the human reference genome (GRCg38/hg38) using BWA[10]. Following the GATK best practices[11], we performed base quality score recalibration and local indel realignment before variant calling. The resulting VCF file was annotated using ANNOVAR[12].

NGS-based deep amplicon sequencing (NGS-DAS)

Amplimers containing the candidate region were PCR-generated using 40 ng of DNA. PCR products were quantified with a Qubit 2.0 Fluorometer (Thermo Fisher Scientific). A 300- to 900-ng amount of DNA was fragmented using NEBNext dsDNA Fragmentase (New England Biolabs) to obtain fragments of approximately 200 bp in size. End repair, ligation of the adapter for Illumina, and sample indexing by a small amplification were then carried out using the NEBNext Ultra DNA library prep kit for Illumina and the NEBNext MultiplexOligos for Illumina Dual Index Primers Set 1 (New England Biolabs). All necessary purifications and size selections to recover only the fragments of interest were done using AMPure XP beads (Beckman Coulter).

Libraries were quality-evaluated using QIAxcel (Qiagen) and quantified with a Qubit 2.0 Fluorometer. The DNA sample libraries were then mixed in equimolecular amounts and sequenced in a MiSeq instrument (Illumina) using the 500-cycle MiSeq reagent kit v2 with a paired-end run of 2 × 250 bp reads. All procedures were performed according to the manufacturer's instructions.

For the bioinformatic analysis, NGS sequencing data were aligned to the reference genome, hg38, using BWA (https://github.com/lh3/bwa). Duplicate reads were marked using Picard MarkDuplicates (version 2.18.6, https://github.com/broadinstitute/picard). Next, GATK 4.1.8.1 (https://github.com/broadinstitute/gatk) was used to calibrate the data, calculate BQSR scores (BaseRecalibrator, ApplyBQSR), and perform variant calling (Mutect2). The resulting VCF files were annotated using Annovar (https://annovar.openbioinformatics.org/en/latest/). Finally, Integrative Genomic Viewer was used to count the number of reads supporting each allele.

Single cell RNA sequencing (scRNAseq): sample preparation and sequencing

Sorted CD8+ cells were centrifuged at 400 x *g* for 5 min at 4 °C, and final concentration and viability were assessed using a TC20™ Automated Cell Counter (Bio Rad) upon staining with Trypan Blue. The sample was encapsulated for a Target Cell Recovery of 6000 cells on the Chromium Controller instrument (10X Genomics), using standard throughput Chromium Next GEM Single Cell 5' Reagent Kit v2 (10X Genomics, PN-1000263). Libraries were prepared following the manufacturer's instructions of protocol CG000331. Briefly, after GEM-RT cleanup, cDNA was amplified during 13 cycles, purified, and quantified on an Agilent Bioanalyzer High Sensitivity chip (Agilent Technologies). To construct the Gene Expression (GEX) library, 10 ng of cDNA were fragmented, end-repaired, A-tailed, and sample-indexed using the Chromium Single Cell 5' Library Construction Kit (10X Genomics PN-1000190) and the Dual Index Kit TT Set A (10X Genomics PN-1000215). Human T cell receptor (TCR) sequences were enriched from the amplified full-length cDNA with the Chromium Single Cell Human TCR Amplification Kit (PN-1000252). Fragmentation, end repair, A-tailing and library indexing of the enriched cDNA were carried out using the aforementioned kits. Finally, the size distribution and concentration of 5' GEX and TCR libraries were verified on an Agilent Bioanalyzer High Sensitivity chip. Sequencing was carried out on a NovaSeq6000 system (Illumina), aiming for approximately 40,000 and 10,000 read pairs per cell for the GEX and the TCR libraries, respectively. The following sequencing conditions were used: 28 bp (Read 1) + 10 bp (i7 index) + 10 bp (i5 index) + 90 bp (Read 2).

Single cell RNA sequencing (scRNAseq): data analysis

The 10x Genomics Cell Ranger software was used for demultiplexing, alignment to GRCh38 human reference genome, filtering, and generation of feature-barcode matrices through unique molecular identifiers (UMIs). Seurat v5.1.0[13], and R v4.4.1 were used for downstream analysis and visualization. Cells containing fewer than 600 features and/or with more than 7% mitochondrial content were considered of low quality and subsequently removed. Estimated doublets were removed using DoubletFinder v2.0.4[14]. The raw count data were normalized with SCTransform, regressing for mitochondrial content and cell cycle phase scoring[15]. Principal Component Analysis was applied to the SCTransform-normalized data to identify significant principal components. These components were then used for constructing a Shared Nearest Neighbor graph. Louvain clustering was applied to this graph to determine cell clusters. Uniform Manifold Approximation and Projection was utilized for the visualization of clusters in a two-dimensional space. Automatic annotation of cells was performed using SingleR v2.6.0[16], and cell types different from CD8 + T cells were removed. After filtering, SCTransform transformation was applied a second time.

To distinguish between cells from the patient and her brother, cells were classified based on specific gene expression. *TNFRSF9* expression was observed in 269 CD8+ T cells. Since scRNAseq does not typically sequence the entire transcript, the somatic reversion could be detected only in a few of those cells, but all cells carrying R1 (8 cells) and R2 (3 cells) variants were classified as male cells (XY) based on the expression of genes located outside the pseudoautosomal region of the Y chromosome. Cells expressing genes located outside the Pseudoautosomal Region (PAR) of the Y chromosome (such as *USP9Y, EIF1AY, TTTY10, TTTY14, KDM5D, RPS4Y1, ZFY, DDX3Y, UTY, TMSB4Y, NLGN4Y, LINC00278, RPS4Y2*, and *PCDH11Y*) were classified as the brother's cells. Conversely, cells expressing the gene XIST were classified as the patient's cells.

The combineTCR function from scRepertoire v2.0.0[17], was used to concatenate clonotype information into an integrated Seurat object. The repertoire landscape was visualized using the built-in functions of scRepertoire.

Cells expressing either one of the genetic variants of interest in *TNFRSF9* were selected using samtools v1.20. To infer the presence of the three specific variants in cells where the target gene (*TNFRSF9*) could not be read directly, a TCR-based proximity approach was employed. Leveraging the clonal nature of TCRs, cells exhibiting the same TCRs—yet lacking direct gene readout—were predicted to also harbor the mutations of interest. This assumption was based on the rationale that cells with identical TCRs have undergone clonal expansion from a common progenitor cell and, therefore, are likely to share genomic mutations present in that progenitor.

Data availability

TNFRSF9 variant hg38 chr1-7920873-G-A (c.730C>T / p.Arg244*) has been deposited in ClinVar under accession number SCV005908025.

Code availability

We used publicly available bioinformatics tools and libraries, as detailed in the "Methods" section.

Received: 2 May 2025; Accepted: 23 October 2025;
Published online: 28 November 2025

References

1. Tangye, S. G., Palendira, U. & Edwards, E. S. J. Human immunity against EBV-lessons from the clinic. *J. Exp. Med.* **214**, 269–283 (2017).
2. Latour, S. & Fischer, A. Signaling pathways involved in the T-cell-mediated immunity against Epstein-Barr virus: lessons from genetic diseases. *Immunol. Rev.* **291**, 174–189 (2019).
3. Somekh, I. et al. CD137 deficiency causes immune dysregulation with predisposition to lymphomagenesis. *Blood* **134**, 1510–1516 (2019).
4. Rodriguez, R. et al. Concomitant PIK3CD and TNFRSF9 deficiencies cause chronic active Epstein-Barr virus infection of T cells. *J. Exp. Med.* **216**, 2800–2818 (2019).
5. Alosaimi, M. F. et al. Immunodeficiency and EBV-induced lymphoproliferation caused by 4-1BB deficiency. *J. Allergy Clin. Immunol.* **144**, 574–583.e5 (2019).
6. Pollok, K. E. et al. Inducible T cell antigen 4-1BB. Analysis of expression and function. *J. Immunol.* **150**, 771–781 (1993).
7. Li, G. et al. 4-1BB enhancement of CAR T function requires NF-κB and TRAFs. *JCI Insight* **3**, e121322, 121322 (2018).
8. Revy, P., Kannengiesser, C. & Fischer, A. Somatic genetic rescue in Mendelian haematopoietic diseases. *Nat. Rev. Genet.* **20**, 582–598 (2019).
9. Miyazawa, H. & Wada, T. Reversion mosaicism in primary immunodeficiency diseases. *Front. Immunol.* **12**, 783022 (2021).
10. Li, H. & Durbin, R. Fast and accurate short read alignment with Burrows-Wheeler transform. *Bioinformatics* **25**, 1754–1760 (2009).
11. McKenna, A. et al. The Genome Analysis Toolkit: a MapReduce framework for analyzing next-generation DNA sequencing data. *Genome Res.* **20**, 1297–1303 (2010).

12. Wang, K., Li, M. & Hakonarson, H. ANNOVAR: functional annotation of genetic variants from high-throughput sequencing data. *Nucleic Acids Res.* **38**, e164 (2010).
13. Hao, Y. et al. Dictionary learning for integrative, multimodal and scalable single-cell analysis. *Nat. Biotechnol.* **42**, 293–304 (2024).
14. McGinnis, C. S., Murrow, L. M. & Gartner, Z. J. DoubletFinder: doublet detection in single-cell RNA sequencing data using artificial nearest neighbors. *Cell Syst.* **8**, 329–337.e4 (2019).
15. Ahlmann-Eltze, C. & Huber, W. glmGamPoi: fitting Gamma-Poisson generalized linear models on single cell count data. *Bioinformatics* **36**, 5701–5702 (2021).
16. Aran, D. et al. Reference-based analysis of lung single-cell sequencing reveals a transitional profibrotic macrophage. *Nat. Immunol.* **20**, 163–172 (2019).
17. Borcherding, N., Bormann, N. L. & Kraus, G. scRepertoire: an R-based toolkit for single-cell immune receptor analysis. *F1000Research* **9**, 47 (2020).

Acknowledgements

We are deeply grateful to the patient and her parents for participating in this study. We would like to thank Rodrigo Martino Bufarull (Hematology, Hospital de la Santa Creu i Sant Pau, Barcelona) for his support in the clinical follow-up of the patient. This work was supported by Instituto de Salud Carlos III, grants PI20/00761 and PI23/00161, co-financed by the European Regional Development Fund (ERDF); and by the Jeffrey Modell Foundation. This research is supported by the European Reference Network for Rare Immunodeficiency, Autoinflammatory and Autoimmune Diseases (ERN-RITA). LB-M is supported by an ISCIII postdoctoral fellowship, "Sara Borrell," CD24/00011, co-financed by the European Union. FC is supported by grants PID2021-125106OB-C32 funded by MCIN/AEI/10.13039/501100011033 and "FEDER Una manera de hacer Europa" and by Agència de Gestió d'Ajuts Universitaris i de Recerca- Generalitat de Catalunya (2021SGR01093). Institutional support to CNAG was from the Spanish Ministry of Science and Innovation through the Instituto de Salud Carlos III and Generalitat de Catalunya through the Departament de Salut and the Departament de Recerca i Universitats. Under direction of the authors, Nerea Moreno-Ruiz provided editing assistance for this publication.

Author contributions

L.B.M. and R.C. conceptualized the study. L.A., M.T., S.R.V., and P.S.P. provided patient care and collected the clinical data. C.F.J., A.A.C., and C.C. performed laboratory analyses and molecular/genetic studies. J.P.P. and M.M.G. were responsible for the flow cytometry studies. L.B.M., F.C., and R.C. analyzed the NGS data (WES, NGS-DAS). M.R.A. provided data and DNA samples from the chimerism monitoring. J.P.P. and A.E.C. analyzed data from scRNAseq. R.C. provided funding support for the study. R.C. and L.B.M. interpreted the overall results and wrote the manuscript. All co-authors reviewed, commented on, and approved the final version of the manuscript.

Competing interests

The authors declare no competing interests.

Additional information

Correspondence and requests for materials should be addressed to Roger Colobran.

Reprints and permissions information is available at http://www.nature.com/reprints

Publisher's note Springer Nature remains neutral with regard to jurisdictional claims in published maps and institutional affiliations.

[1]Translational Immunology, Vall d'Hebron Research Institute (VHIR), Vall d'Hebron Barcelona Hospital Campus, Barcelona, Catalonia, Spain. [2]Jeffrey Modell Diagnostic and Research Center for Primary Immunodeficiencies, Barcelona, Catalonia, Spain. [3]Centro Nacional de Análisis Genómico (CNAG), Barcelona, Catalonia, Spain. [4]Hospital Clínic de Barcelona, Muscle Research and Mitochondrial Function Group, IDIBAPS, and CIBERER, Barcelona, Catalonia, Spain. [5]University of Barcelona (UB), Barcelona, Catalonia, Spain. [6]Immunology Division, Hospital Universitari Vall d'Hebron (HUVH), Vall d'Hebron Barcelona Hospital Campus, Barcelona, Catalonia, Spain. [7]Department of Cell Biology, Physiology and Immunology, Autonomous University of Barcelona (UAB), Bellaterra, Catalonia, Spain. [8]Immunology Department, Laboratori Clínic ICS Camp de Tarragona, Hospital Joan XXIII, Tarragona, Catalonia, Spain. [9]Department of Clinical and Molecular Genetics, Hospital Universitari Vall d'Hebron (HUVH), Vall d'Hebron Barcelona Hospital Campus, Barcelona, Catalonia, Spain. [10]Immunohematology Laboratory, Banc de Sang i Teixits (BST), Barcelona, Catalonia, Spain. [11]Infection and Immunity in Pediatric Patients, Vall d'Hebron Research Institute (VHIR), Vall d'Hebron Barcelona Hospital Campus, Barcelona, Catalonia, Spain. [12]Pediatric Infectious Diseases and Immunodeficiencies Unit, Children's Hospital. Hospital Universitari Vall d'Hebron (HUVH), Vall d'Hebron Barcelona Hospital Campus, Barcelona, Catalonia, Spain. [13]Departament of Genetics, Microbiology and Statistics, Faculty of Biology, Universitat de Barcelona (UB), Barcelona, Catalonia, Spain. [14]Institute of Biomedicine of the University of Barcelona (IBUB), University of Barcelona (UB), Barcelona, Catalonia, Spain. [15]Instituto de Salud Carlos III, Centro de Investigación Biomédica en Red de Enfermedades Raras (CIBERER), Barcelona, Catalonia, Spain. [16]Institut de Recerca Sant Joan de Déu (IRSJD), Barcelona, Catalonia, Spain. [17]Hematology Department, Hospital de la Santa Creu i Sant Pau. IIB-Sant Pau and Josep Carreras Leukemia Research Institute. Departament de Medicina, Universitat Autònoma de Barcelona (UAB), Barcelona, Catalonia, Spain. [18]Clinical Immunology and Primary Immunodeficiencies Unit, Allergy and Clinical Immunology Department, Hospital Sant Joan de Déu, Barcelona, Catalonia, Spain. [19]Study Group for Immune Dysfunction Diseases in Children (GEMDIP). Institut de Recerca Sant Joan de Déu (IRSJD), Barcelona, Catalonia, Spain. [20]Departament de Cirurgia i Especialitats Médico-quirúrgiques, Universitat de Barcelona (UB), Barcelona, Catalonia, Spain. ✉e-mail: roger.colobran@vallhebron.cat